Journal of Energy Storage 114 (2025) 115799

Contents lists available at ScienceDirect

Journal of Energy Storage

journal homepage: www.elsevier.com/locate/est

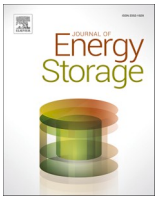

Research Papers

Numerical analysis of solidification of paraffin-type PCMs by using customary fixed-grid methods

Milad Tajik Jamal-Abad [a,*], Arnold Martínez [b], Mauricio Carmona [b], Cristóbal Cortés [a]

[a] Institute of Energy and Resources Efficiency of Aragón (ENERGAIA), University of Zaragoza, 50018 Zaragoza, Spain
[b] Mechanical Engineering Department, Universidad del Norte, Km 5 Antigua Via Puerto Colombia, Barranquilla, Colombia

ARTICLE INFO

Keywords:
Phase change material
DSC
Solidification
Numerical simulation
Apparent heat capacity

ABSTRACT

A numerical study is conducted to predict temperature measurements during the solidification of a commercial paraffin-type PCM in a vertical cylinder under T-history conditions. Two fixed-grid techniques are implemented: the enthalpy-porosity formulation and the Apparent Heat Capacity (AHC) method. As it is known, the first, originally devised for metals and alloys, raises questions about its applicability to other materials. Additionally, there may be uncertainties surrounding the assignment of internal parameters when representing the transitional "mushy" region. On the other side, there are limited publications that utilize the AHC method, and even fewer have addressed and compared both methods. Phase-change properties of the paraffin material are determined through the use of differential scanning calorimetry (DSC): phase change temperature range, latent heat, and specific heat capacity vs. temperature curve ($c_p - T$). Results show that there is significant disagreement between measurements and simulation results for both methods. The enthalpy-porosity technique may not be entirely suitable for accurately modeling phase changes in paraffin-type PCM. Furthermore, while the AHC method can effectively predict the initial and final stages of solidification, it tends to struggle with accurately simulating the mushy zone. An interesting observation is that in the AHC method, the cooling rate is a critical factor influencing the accuracy of solidification simulations and results depend very much on the DSC $C_p - T$ curve introduced, determined under a constant cooling rate, which is indeed variable during the experiment

1. Introduction

Phase change materials (PCMs) have a strong capacity for energy storage and are distinguished by their ability to maintain a consistent temperature during the absorption or release of heat. Various studies have been conducted to investigate the heat transfer and phase change phenomenon in the context of inward solidification processes. Cylindrical and spherical encapsulated PCMs are favored in thermal energy storage (TES) applications due to their advantageous volume-to-surface area ratio [1,2]. Extensive research has been carried out to gain a deeper insight into the phase change mechanisms within these encapsulated PCMs. This knowledge is crucial for achieving precise thermal designs in TES systems. Nevertheless, the majority of research efforts have predominantly concentrated on the melting process [3–5]. However, it is equally crucial to comprehend the solidification dynamics of encapsulated PCMs in order to effectively analyze the discharge of stored energy.

Extensive researchers have explored the solidification of PCMs within a range of encapsulation geometries, including spheres [6–8], rectangular enclosures [9,10], and horizontal cylinders [11–13]. Shaker et al. [14] investigated the factors affecting the melting and solidification characteristics of a cylindrical encapsulated PCM (EPCM) using two different PCMs, Lauric acid and paraffin wax. They discovered that paraffin wax stored significantly more energy than Lauric acid under identical heat transfer fluid (HTF) conditions. Darzi et al. [15] conducted a numerical study on the melting and solidification of a PCM in various horizontal annulus configurations, including circular and elliptical cylinders. They found that natural convection plays a significant role in the melting process, and the addition of nanoparticles to the base PCM enhances both the melting and solidification rates. Additionally, inserting fins significantly improved the melting and solidification rates, particularly during the solidification process. Alsulami et al. [16] examined the solidification of a PCM-filled concentric cylindrical annulus subjected to internal heat generation. They demonstrated that various parametric variables have a critical influence on the solidification process. Afsharpanah et al. [17] explored the combination of several enhancement techniques, such as porous foams, fins, and

* Corresponding author.
E-mail address: mtajikjamalabad@unizar.es (M.T. Jamal-Abad).

https://doi.org/10.1016/j.est.2025.115799
Received 25 September 2024; Received in revised form 16 January 2025; Accepted 9 February 2025
Available online 13 February 2025

nanomaterials, to minimize the charging time of cylindrical cold thermal energy storage enclosures. Their results showed that using copper foam with 0.95 porosity and CuO nanomaterials at a 0.03 concentration simultaneously led to a 92.5 % increase in the phase change rate. Mahamudur et al. [18] carried out an experimental study to explore the impact of cylinder size, thermal loading, and the inclusion of graphene additive on the melting and solidification dynamics of PCM within a millimeter-scale vertical cylinder. Oztop et al. [19] explored a novel approach to enhance the solidification of PCM, evaluating the impacts of cooler shape and placement in a molten PCM-filled enclosure. They found that the shape and positioning of coolers within PCM cavities had a significant impact on solidification rates. The effects of PCM container geometry on the melting and solidification rates were investigated by Hekmat et al. [20]. The container geometries studied included circle, horizontal ellipse, vertical ellipse, square, triangle, and downward and upward trapezoids. The results showed that the best performance in melting was achieved with the downward trapezoid, while the horizontal ellipse provided the best performance in solidification. In another study, Izgi and Arslan [21] numerically investigated the solidification of PCM within a vertical cylindrical enclosure using a three-dimensional transient simulation conducted with ANSYS-Fluent. The study examined the effects of various parameters, including natural convection, initial superheating temperature, encapsulation size, and the heat transfer coefficient at the capsule's outer surface. Their findings revealed that natural convection plays a significant role during the initial stages of solidification, after which conduction becomes the dominant mode of heat transfer. Additionally, the results indicated that the cavity diameter significantly influences the freezing process, whereas variations in cavity height have a negligible impact.

Computational Fluid Dynamics (CFD) is an effective method for addressing complex, nonlinear problems involving the simultaneous transfer of mass, heat, and momentum [22]. It is commonly applied to simulate the thermal behavior of PCMs by using commercial software, such as COMSOL Multiphysics and ANSYS Fluent. Notably, Chiu and Martin [23] as well as Mosaffa et al. [24] explored the potential of various PCMs, employing COMSOL Multiphysics to model phase change. In a separate study, Ye et al. [25] utilized Ansys Fluent software to delve into fluid flow and heat transfer within a plate-fin unit, which was applied for swift heat storage and release facilitated by paraffin.

Although a proper numerical formulation of the problem would demand the tracking of the moving liquid-solid interface, the ensuing high computational load has prevented this approach in common studies. So-called fixed-grid models are used instead. Many researchers have utilized the Solidification and Melting model in ANSYS Fluent to simulate phase change phenomena [26]. This model is based on the enthalpy-porosity method, a widely employed technique for modeling phase change processes. In recent years, substantial research efforts have been dedicated to utilizing this model, yielding valuable agreements with experimental findings. Riahi et al. [26] proposed a novel geometry incorporating fins to increase the heat transfer area and PCM mass, which outperformed the efficiency of traditional metal fins. They implemented this design using ANSYS Fluent. Vahidhosseini et al. [27] utilized ANSYS Fluent for a numerical parametric comparison of latent heat storage (LHS) units with PCM and various thermal fins during the charging and discharging processes. Kheirabadi et al. [28] used ANSYS Fluent software to analyze the impact of the mushy zone constant and the melting temperature range on phase change heat transfer. The effects of different fin arrangements on the melting behavior of PCM-based paraffin wax within a square cell were numerically investigated by Rashid et al. [29], who employed ANSYS Fluent for transient numerical simulations. The Apparent Heat Capacity (AHC) method is an alternative approach which can also be implemented in Ansys Fluent by incorporating the C_p-temperature relationship acquired from Differential Scanning Calorimetry (DSC). It's important to note that to attain accurate results, the scanning rate in the DSC analysis should align with the cooling rate or heating rate pertinent to the selected application, as emphasized in the findings of Iten et al. [30]. Researchers such as Raj and Velraj [31] and Diarce et al. [32] have successfully employed the Apparent Heat Capacity method in Ansys Fluent, demonstrating commendable agreements with experimental data.

As far as the authors are aware, only a few publications discuss the implementation of the AHC method within ANSYS Fluent. The enthalpy-porosity model employs a linear interpolation for the liquid fraction within the temperature range of solidus to liquidus. However, it is acknowledged that the phase transition actually exhibits a non-linear behavior as pointed out in reference [33]. The AHC method offers a means to capture this effect, as the specific heat capacity's curve shape and position hold insights into the nature of the phase transition phenomenon. Kheirabadi et al. [34] offer a comparison between the AHC method and the enthalpy-porosity model in COMSOL software. Additionally, Iten et al. [35] conducted a similar comparison, but omitted the consideration of gravity's influence and recommended the utilization of the AHC method, as both models demonstrated favorable agreement. Reichl et al. [36] employed Ansys Fluent to simulate the two-dimensional Stefan problem. They conducted a comparative analysis of results obtained using both the AHC and the enthalpy-porosity methods. Their simulation considered natural convection incorporating the Boussinesq approximation and the alternative of a temperature-dependent liquid density. The authors prefer employing the AHC modeling approach in conjunction with the Boussinesq approximation, suggesting that this approach can be particularly effective, provided the heat capacity curve is accurately represented. This choice helps avoiding uncertainties associated with selecting the mushy zone constant, a decisive parameter of the enthalpy-porosity technique. Ouali et al. [37] applied the apparent heat capacity approach to model phase transition processes in PCM, where the PCM heat capacity is expressed as a temperature-dependent function. This method can be easily integrated into various software to assess the energy efficiency of latent storage systems. In another study [38], the thermal gradients inside a composite material during a non-isothermal phase change process were numerically evaluated and analyzed using a physical model based on the apparent heat capacity approach.

This research aims to address these issues by conducting a systematic investigation into the utilization of thermophysical property values determined via calorimetry (DSC) in numerical models of the solidification process for a paraffin-type PCM within cylindrical containers. In the experiment, cooling is restricted to assure a low heat transfer rate, and thus a cross-sectionally uniform temperature, which is commonly known as a T-history experiment. The cooling process is simulated using the enthalpy-porosity and $C_p - T$ methods implemented in the Ansys Fluent 2020 R2 [37]. Values of temperature predicted along time are compared in detail with those measured. The study incorporates experimental values of phase-change properties determined by DSC, along with other measured material properties. It also examines the impact of variations in some of these properties, as well as the effect of other internal parameters of the phase-change models, on the simulation results. The paper develops a detailed discussion on the differences observed and how they vary with model parameters, attempting to explain them in physical terms. The research endeavors to provide a more rigorous and well-founded approach to the exploration of possible modeling expedients to improve this kind of simulations. Also, the possible implications for the numerical modeling of practical PCM applications, larger and quicker than T-history experiments, is tentatively discussed.

2. Experimental work

2.1. Determination of thermophysical properties by DSC

The commercial paraffin RT45 distributed by Rubitherm Technologies GmbH was adopted as the material for the experiment. It has a melting temperature range of 41 °C to 46 °C. The DSC technique was

employed to determine the latent heat of fusion, the start and end temperatures of the phase change, and the specific heat values.

Calorimetry was performed using the DSC 250 equipment from the Discovery series, equipped with an RCS90 refrigeration system enabling tests to be conducted within a range of 90 °C to 550 °C. The experiments involved 5 to 6 mg of RT45 under a nitrogen atmosphere with a flow rate of 50 ml/min. The DSC 250 operates within a temperature range starting from 180 °C, with an accuracy of ±0.05°C and a temperature precision of ±0.008°C. DSC measures the quantity of heat absorbed or released by a sample as its temperature changes. This is achieved by monitoring the temperatures of both the sample and a reference material simultaneously. The disparity in temperature is then utilized to calculate the heat flow between the sample and the oven [40].

The assessment of thermophysical properties in Phase Change Materials poses certain challenges from an experimental perspective. This is because PCMs can exhibit phenomena like subcooling, hysteresis, and crystallization, all of which can complicate the interpretation of the determined values. In calorimetry, there is the issue of working with relatively small sample sizes, and discrepancies in results may arise from the poor homogeneity of the material. Furthermore, it is important to note that the outcomes may vary depending on the specific heating or cooling rates used during the tests. The experimental evaluation of thermophysical properties followed the guidelines specified in the ASTM D4419 standard [41], with heating rates of 20, 10, 5, and 1°C/min applied. A more detailed description of the procedure is provided in [42]. Additionally, the ASTM E1269 standard [43] was employed to determine the specific heat values.

The experimental results of DSC are illustrated in Fig. 1. Vertical axis is the normalized heat flow which is calculated by dividing it by the corresponding sample mass for each experiment. The heat flow exhibits noticeable variations with changes in the heating rate, including a shift in the peak of the transition and in the initial and final values of the phase change. In order to identify the beginning and end of the phase change, the enthalpy, and the phase change temperature, this figure should be interpreted. Two distinct peaks are observed during the heating process: a smaller peak, corresponding to a solid-solid phase change occurring at temperatures between 20 and 30 °C, and a higher peak between 40 and 50 °C, which represents the material's melting point where the phase transition from solid to liquid takes place. The initial point of the phase transition is determined as the point where the tangent intersects the baseline of the extrapolated sample and the maximum upward slope of the peak. Similar process is used for determining the end of the phase change. The latent heat of fusion L (kJ/kg) is calculated by integrating the heat flow curves over time, from the start to the end of the primary peak. In Fig. 2, the specific heat is calculated using the heat flow and the temporal variation of sample temperature. Two solid-phase transformations are discernible before fusion takes place. It's notable that at lower heating rates, the specific heat peak becomes progressively more pronounced, approaching a state of thermodynamic equilibrium. A subtle shift towards the left is observed during heating, while during cooling, the curves exhibit a contrasting shift to the right.

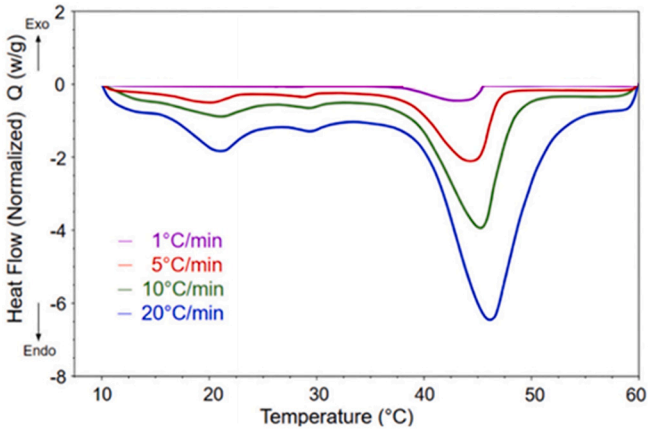

Fig. 1. Results of the DSC for heating rates from 0.5 – 20°C/min.

It's important to highlight that paraffins commonly demonstrate multiple solid phases, as illustrated in Figs. 1 and 2. These transitions arise from alterations in molecular chain structure, geometry, and interactions, typically involving relatively low transition enthalpies, as evident in the figures. This complexity in solid phase behavior underscores the intricacies that must be considered when modeling paraffin-type PCMs.

To determine the thermophysical properties via calorimetry, a method involving five tests was employed. These tests were conducted at heating rates between 1 and 20 °C /min. The average values for each property can be found in Table 1. To calculate the latent heat of fusion (L), each experiment was repeated three times. The standard deviation of the solidus temperature (T_s) was found to be 0.4, 0.1, 0.05, and 0.04, respectively, for heating rates of 1, 5, 10, and 20 °C/min. Similarly, for the liquidus temperature (T_l), the standard deviations were 0.06, 0.25, 0.26, and 0.19 for the corresponding heating rates. Additionally, the details of the property values presented in Table 1 are described in [5,42]. Higher heating rates lead to greater thermal gradients within the PCM, causing the material to experience thermal lag. This delays the phase change and shifts the liquidus temperature upwards

2.2. Experimental setup

Fig. 3 shows a photograph and a sketch of the experimental setup of the trial. The cooling tests were based on the setups used for T-history experiments. Test tubes with an internal diameter of 1.26 cm and a height of 15 cm were used, which were filled to a height of 13 cm with distilled water and liquid PCM RT45. The temperature inside the tubes is monitored by means of type K thermocouples located 5 cm from the lower base. To minimize heat loss, thermocouples with small diameters and insulated wires are used to reduce heat exchange at the junction. For the experiments, a thermal bath was set up with a temperature of 50 °C. Once the temperature of the medium had stabilized, the water and PCM samples were submerged until reaching thermal equilibrium. When the temperatures inside the samples stabilize, the test tubes are quickly removed and placed in cylindrical insulating shells made of polystyrene foam, in order to assure a low cooling rate and thus a uniform temperature profile in the cross-section, as corresponding to a T-history experiment. As a result, the phase change process occurs under more controlled conditions, leading to more accurate results with minimal environmental disturbances. Two identical test tubes filled with PCM are used in order to assure homogeneity of the material and uniformity of cooling conditions; the corresponding temperature curves were indistinguishable. The T-history method is relies on the lumped capacitance model, uniform temperature distribution is assumed within the sample. All thermocouples were calibrated using a constant temperature bath within the working temperature range. The uncertainty values are determined as follows: ±0.2% for dimensions, ±4% for the K-type thermocouple, ±2.5% for solidification time, and ±6% for latent heat.

Temperatures inside the water, the PCM and the environment surrounding the specimens are monitored throughout the cooling process. Fig. 4 shows the cooling curves. Rapid cooling is evident in the sensible heat region of the liquid PCM while it reaches the solidification temperature. Subsequently, upon reaching the phase change region, there is a slower cooling between the liquidus and solidus temperatures, when the latent heat is released. At this stage it is possible to see that the cooling of the reference substance (water) is greater than that of the PCM, corresponding to an approximately constant heat capacity. The initial faster temperature drop observed in the PCM is due to its relatively high thermal conductivity in the early stages of cooling before the

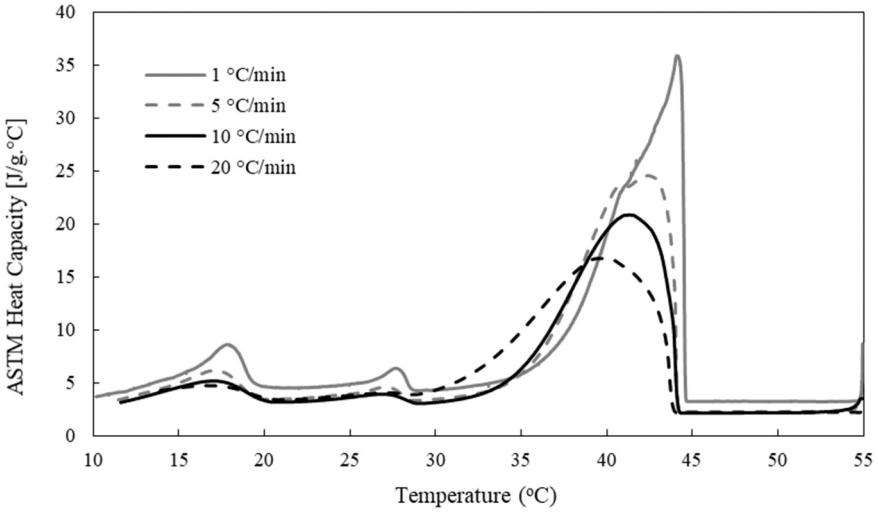

Fig. 2. Specific heat results according to ASTM procedure.

Table 1
Thermophysical properties at different heating rates were used for the numerical simulation.

Heating rate ($^{\circ}C/min$)	Supplier/n.a	20	10	5	1
T_s (^{o}C)	41	40	39	38.6	38.4
T_l (^{o}C)	46	50.9	50.9	46.9	45.6
$T_m(main\ peak)$ (^{o}C)	44	46.3	43.6	44.6	43.6
L (kJ/kg)	160	121.73	126.14	129.56	133.37
k_l $(W/m.K)$	0.2	0.156			
k_s $(W/m.K)$	0.2	0.234			

phase change occurs, whereas water cools more steadily without undergoing any phase change.

3. Numerical modeling

3.1. Physical and numerical models

Two types of numerical analyses are conducted. Firstly, a comprehensive model that includes all the domains of the experimental setup: fluid within the test tube, glass, thermal insulation, and a simplified representation of the enclosure. The latter is an axisymmetric (2D) approach to the real geometry, wherein external heat transfer (natural convection in air and heat radiation to surfaces) is simulated. This model is used to adjust the heat transfer external to the test-tube, essentially, the emissivity of the surface of the insulation, which is a critical parameter under the conditions of the experiment, and largely unknown. Only water is simulated, since the complexity of the phase change computations (by either of the two models) prevents using such a comprehensive model for that. Instead, a simplified model is developed encompassing only the PCM material and with the external heat transfer represented by boundary conditions of the "convective" type directly on its surface.

The comprehensive model, represented in Fig. 5, comprises an axisymmetric computational domain of 14,976 cells, with 1150 corresponding to the fluid domain of the specimen. Its dimensions, akin to those of the real container, were confirmed by enlarging them progressively until no appreciable variation of the results obtained. Non-slip is imposed for flow over all solid walls and the aperture (the space between the container and the test tube) is represented by the output boundary condition, which allows air flow in both directions. External walls are approximated as adiabatic, with all the heat being evacuated by the natural air flow through the aperture.

Initially, both the tube and the sample are assumed to be at a uniform temperature, which is higher than the phase change temperature of the PCM. The rest of the assembly (container walls) is initially at a temperature equal to the controlled room temperature, which is set to a constant value. Given the conditions, air and water flows are reasonably assumed laminar. Incompressible flow is simulated inside the test tube

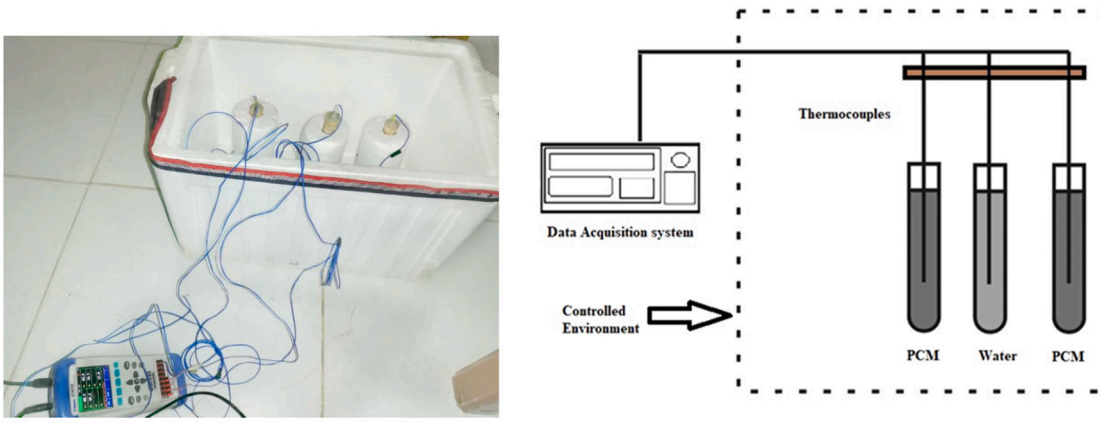

Fig. 3. a) T-history Experimental setup, b) Scheme of the experimental setup

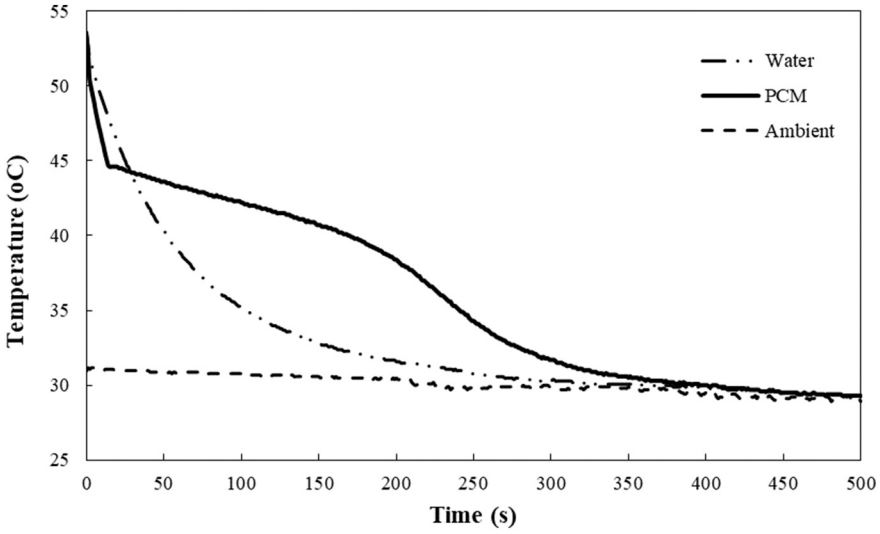

Fig. 4. Experimental results of the cooling curves of PCM and water

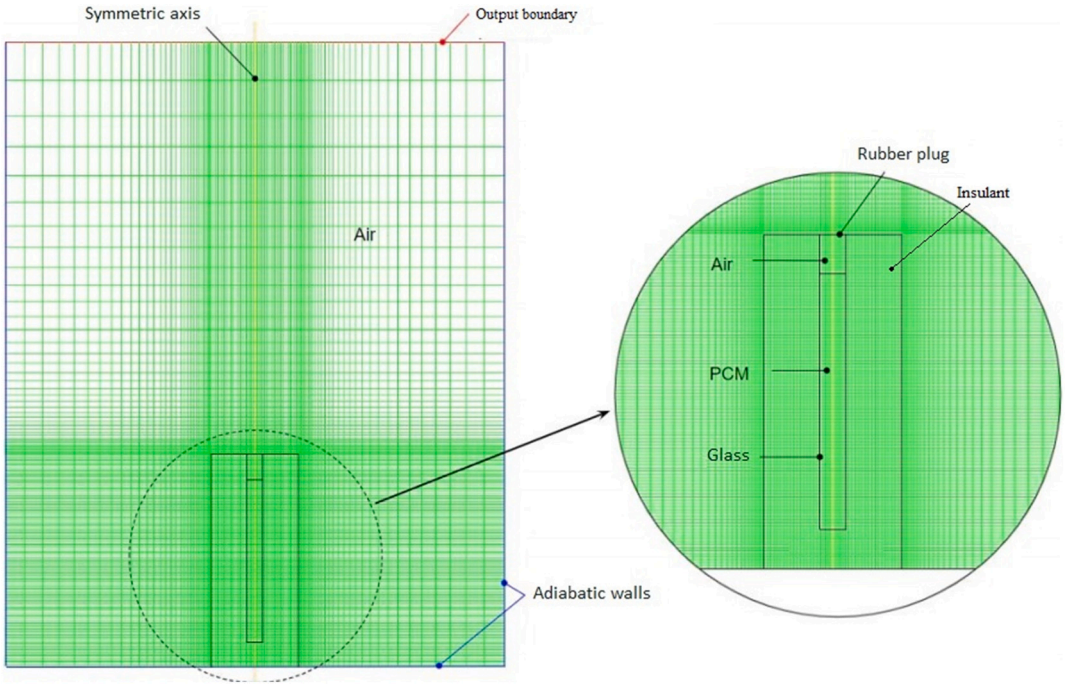

Fig. 5. Boundary conditions and meshing of the comprehensive model.

and within the cavity via the conservation equations of mass, momentum and energy. Density is assumed constant, and buoyancy is imposed via the Boussinesq approximation in which $\rho = \rho_0(1 - \beta\Delta T)$, where ρ_0 is the reference density in the solid phase 880 kg/m^3, and β is the thermal volumetric expansion coefficient.

Since the heat transfer rate is very small under the conditions of the experiment, IR radiation has to be forcibly accounted for, even at such low temperatures. Surfaces of the insulant and the container are assumed reasonably diffuse-gray, and of equal emissivity. The Fluent's so-called Surface to Surface (S2S) model is used, which implements the radiative transfer equations between opaque surfaces, and adopts an efficient scheme for computing view factors. The external radiation boundary condition is imposed in the aperture, which amounts to considering it black at ambient temperature.

Fig. 6 illustrates the computational cooling curve obtained alongside the experimental result. Simulations were repeated for different values of the emissivity, that of 0.6 leading to very good agreement, the error being <1.0 % at all times.

To study the phase change models for the PCM with a reduced computational cost, a simplified model has been used. The simplified thermal model is based on two-dimensional heat transfer within a cylindrical container, as depicted in Fig. 7. Only the sample (PCM or water plus the space filled with air above) is numerically simulated, assuming axisymmetric conditions, incompressible laminar flow and the Boussinesq approximation. External heat transfer is represented by a "convective" type of boundary condition on the external surfaces of this sample. This comprises conduction in the solids and external air natural convection and radiation between surfaces, as shown by the equivalent thermal circuit in Fig. 7. The thermal contact resistance at the interface between the tube and insulation was assumed negligible based on the high contact quality achieved during assembly and the relatively low

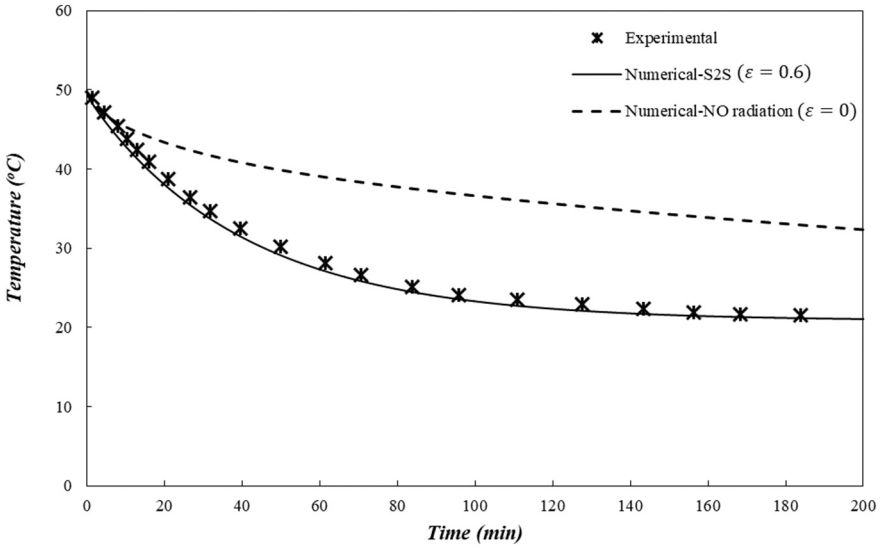

Fig. 6. Validation of the comprehensive model for water.

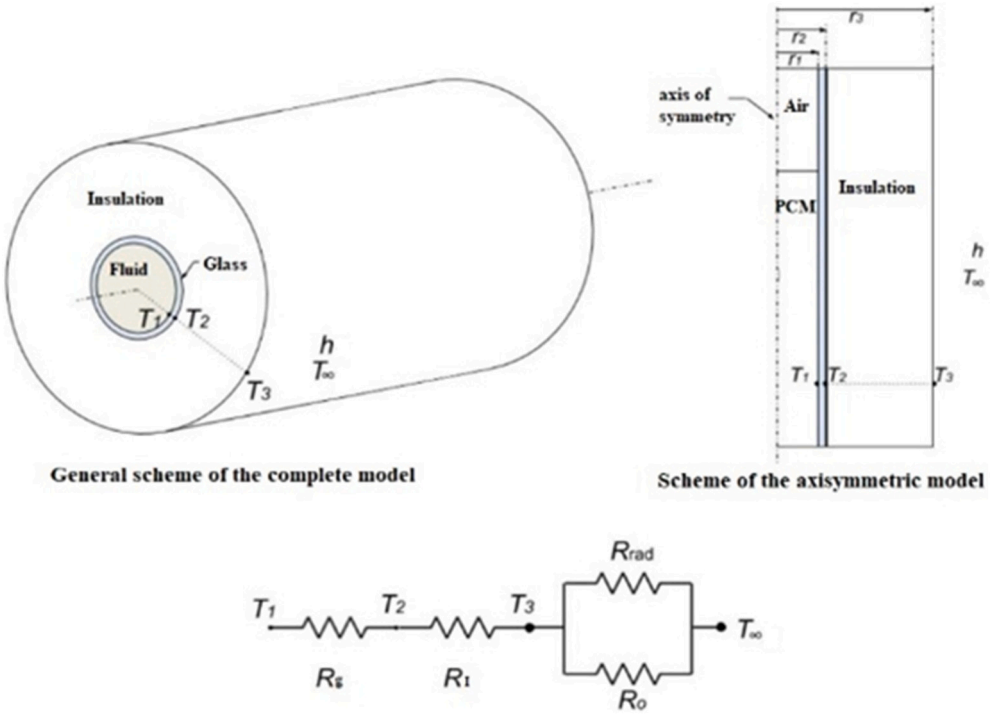

Fig. 7. The schematic view of the thermal model illustrating the wall boundary condition for the simplified model.

thermal conductivity of the insulation material, which dominated the overall resistance.

Constant properties of the air and materials were used in the calculation, as well as the surface emissivity determined by the comprehensive modeling. Customary heat transfer formulas for heat conduction, natural convection from vertical surfaces and heat radiation from diffuse-gray surfaces to a large cavity were employed [44]. Radiation, and also to a lesser degree natural convection, depend on surface and ambient temperatures, but given the low cooling rate, it was considered that constant transfer coefficients will provide enough accuracy. For this, average surface temperatures, as given by the comprehensive model, were used.

A 2D axisymmetric computational domain was established, incorporating two distinct fluid regions: one containing air and the other comprising the working substance, either water or PCM. The rubber plug at the upper part was modeled using a thin-wall thickness approach with the same convective boundary condition applied to it.

The solidification process was simulated using the ANSYS Fluent 2022 R2 code. The conservation equations for mass and momentum were solved using the SIMPLE algorithm. Momentum and energy equations were discretized with a second-order Upwind scheme, while pressure correction was performed using the PRESTO! (PRESsure STaggering Option) method. Relaxation factors of 0.3, 0.7, and 1 were applied to pressure, momentum, and energy, respectively. Convergence of the solution was verified at each time step throughout the simulation. These modeling choices are consistent with recommendations from the literature [5,45]. The simulations were conducted with a time step of 0.3 s. This value was chosen based on a preliminary sensitivity analysis

to ensure numerical stability and accuracy, while maintaining computational efficiency. The maximum number of iterations per time step was set to 80. This value was selected to allow for convergence within each time step without excessive computational overhead

Fig. 8 shows a comparison of the three curves corresponding to the cooling of water: experimental, comprehensive model and simplified model. The excellent agreement indicates that the approximate representation of heat losses in the simplified model is adequate. This achievement has resulted in a significant reduction in computational cost, enabling detailed studies of the phase-change models.

3.2. Phase-change models

3.2.1. Enthalpy-Porosity method

The enthalpy-porosity technique is widely used for simulating melting and solidification processes within PCM enclosures, especially in scenarios where natural convection significantly influences the phase change behavior. This method is particularly suitable for handling phase transitions within a fixed computational domain. To account for these transitions, the momentum equation is modified to ensure zero velocities in the solid phase. A typical approach involves introducing a high-magnitude source term (S_u) into the momentum equation, effectively damping motion in solid regions and accurately representing the phase change dynamics. The mass conservation equation:

$$\frac{\partial \rho}{\partial t} + \nabla.(\rho V) = 0 \tag{1}$$

The momentum conservation equation is:

The Carman-Kozeny equation provides an expression for the hydraulic conductivity, which is used in conjunction with Darcy's law to model flow resistance in a porous medium. This approach is applied in the momentum equation to account for the drag force in the mushy region [46].

$$\frac{\partial(\rho V)}{\partial t} + \nabla.(\rho V) = -\nabla \mathrm{p} + \mu \nabla^2 V + \rho g + S_u \tag{2}$$

where ρ is density, and μ is dynamic viscosity. The term S_u modifies the momentum balance depending on the phase. The source term S_u is dynamic, varying according to the local phase state of the material. It adopts a high value in the solid region, ensuring complete immobility by suppressing any velocities. As the material transitions into the liquid state, the magnitude of the source term gradually decreases, eventually approaching zero when the material is fully liquid. This gradual variation effectively models the phase transition process by accommodating the changes in flow resistance within the computational domain. It is defined as

$$S_u = -\frac{C(1-\gamma)^2}{\gamma^3 + \varepsilon} u_i \tag{3}$$

where γ is the liquid volume fraction ("porosity") and C is a constant, commonly known as the "mushy" zone constant, which is the region where the liquid fraction ranges from 0 to 1, and thus contains a mixture of phases. C varies according to its morphology, and thus on the flow details. Higher values of C result in stronger velocity damping, leading to a thinner mushy region and approaching a situation resembling that of a pure substance. The constant ε is introduced to prevent numerical division by zero.

Voller [47] initially introduced the enthalpy-porosity technique to address phase change problems related to convective-diffusion controlled heat transfer. The energy equation can be written as:

$$\frac{\partial \rho H}{\partial t} + \nabla.(\rho V H) = \mathrm{k}\nabla^2 \mathrm{T} \tag{4}$$

The governing energy equation thereby contains one enthalpy H that includes latent and specific heat

$$H(T) = \int_{T_m}^{T} C_p dT + \gamma L \tag{5}$$

where C_p the specific heat and L the latent heat of the PCM. L is associated with the liquid fraction, γ, that allows the computation of the change in enthalpy from the energy in the material during the phase change [39]. The general form of γ is written as

$$\gamma = \begin{cases} 0 & \text{if } T < T_s \\ \dfrac{T - T_s}{T_l - T_s} & \text{if } T_s < T < T_l \\ 1 & \text{if } T > T_l \end{cases} \tag{6}$$

In this formulation, the liquid fraction γ within a given element is thus related to the enthalpy balance through a linear relationship with the liquidus and solidus temperatures. The liquid fraction is recalculated for each iteration.

3.2.2. Apparent heat capacity method (AHC)

The Apparent Heat Capacity (AHC) Method models the thermal behavior of phase change materials by incorporating the effects of enthalpy variation during phase transitions. In this method, the phase change enthalpy's impact is incorporated into the temperature-

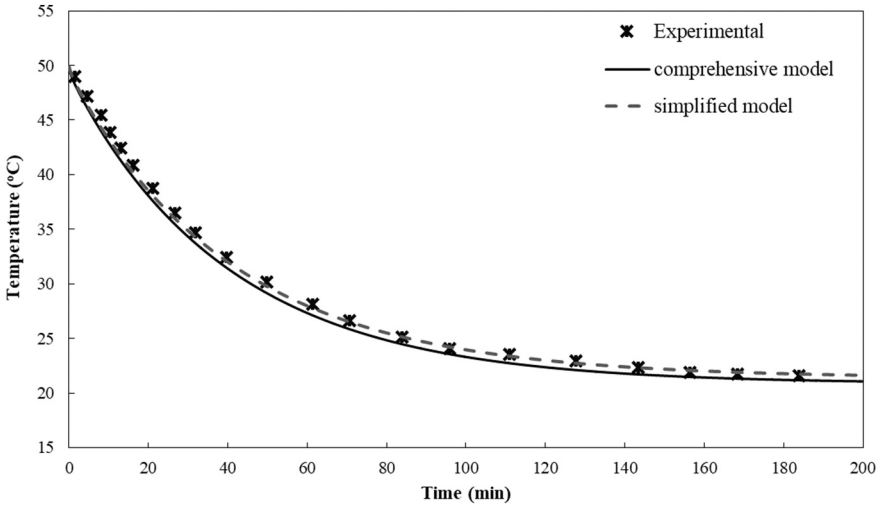

Fig. 8. A comparison of the three water cooling curves: experimental data, comprehensive model and simplified model.

dependent heat capacity by raising the heat capacity during the phase transition [48]. The time-derivative of the enthalpy in this approach is calculated as follows [49]:

$$\frac{\partial H}{\partial t} = \frac{\partial H}{\partial T}\frac{\partial T}{\partial t} \tag{7}$$

where $\frac{\partial H}{\partial T} = \rho C_p(T)$ represents the temperature-dependent apparent heat capacity.

The apparent heat capacity can be determined using DSC, although the results are highly sensitive to variations in heating and cooling rates. The approach is straightforward: the specific heat capacity curve, obtained from DSC as a function of temperature ($C_p - T$) (Fig. 2), is utilized as the variable specific heat capacity of the material in ANSYS FLUENT software.

The AHC was used initially to solve pure diffusion problems, i.e., ignoring the movement of the liquid phase by differences of density, which in absence of a variable density leads to a conduction problem. Since convection is incorporated into the enthalpy-porosity model and is likely to play a significant role in the problem of this research, the following generalization is employed [50,51]. The technique of a source term S_u in the momentum equation will relate linearly the enthalpy with the liquid fraction and thus lead to numerical results similar to those of the enthalpy-porosity method. Instead, we model a liquid with a viscosity that varies with temperature according to our measurements [5] on the liquid PCM above the solidus point, and below we fair a temperature function reaching a significantly high value. This assures that velocity of the medium decreases in the mushy region and finally stops when it is a solid.

$$\mu_l = \begin{cases} -\left(2.273\times10^{-1}\right)T + 33.83 & T \le T_s \\ \left(2.283\times10^{-7}\right)T^3 - \left(3.501\times10^{-5}\right)T^2 + \left(1.73\times10^{-3}\right)T - 0.02587 & T > T_s \end{cases} \tag{8}$$

The apparent heat capacity method embeds the latent heat contribution directly into a modified heat capacity curve $C_p(T)$, which includes both sensible and latent heat effects. This approach simplifies the numerical treatment by removing the need for a separate source term, as seen in the enthalpy-porosity method. From a physical perspective, the enthalpy-porosity method explicitly tracks the liquid fraction and latent heat, offering a more detailed representation of phase change dynamics. In contrast, the apparent heat capacity method integrates these effects into a single curve, which simplifies the implementation but may obscure some physical details. While the two methods are mathematically equivalent under steady conditions, their practical implications differ depending on the complexity of the phase change process and the desired level of physical insight.

4. Numerical results

4.1. Grid independence

Various element sizes were tested by comparing the results with experimental data over the entire process duration to ensure that the solution is independent of the adopted grid density. Structured meshes with 65,844, 23,800, 6120, and 2332 quadrilateral elements were employed. The meshes employed were uniform, with quadrilateral elements of similar size throughout the computational domain. Fig. 9 illustrates the comparison between experimental results and simulations using water as the working fluid for different mesh sizes. In this figure, a strong agreement is observed between the experimental data and the numerical model. Clearly, there are no significant differences in the simulated cooling curves across the different mesh sizes when compared to the experimental results. For those 4 meshes, the same behavior is observed for the numerical model of PCM phase change by either of the two methods. Fig. 10 represents the result for the enthalpy-porosity method.

4.2. Validation against experiment and comparison of phase change models

Fig. 10 represents the PCM numerical cooling curve predicted by the enthalpy-porosity method, the simulations were conducted using a mushy region constant value of 10^5 and the PCM properties provided by

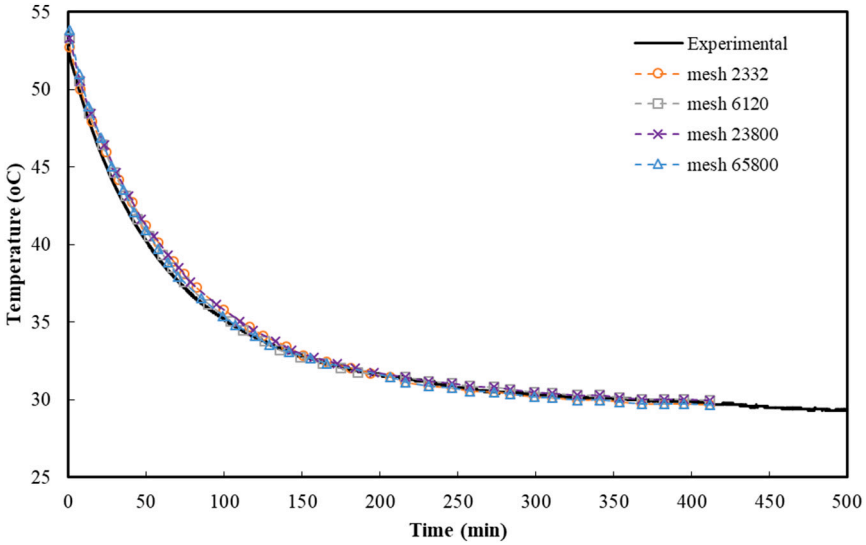

Fig. 9. Results of the validation of the numerical model for water

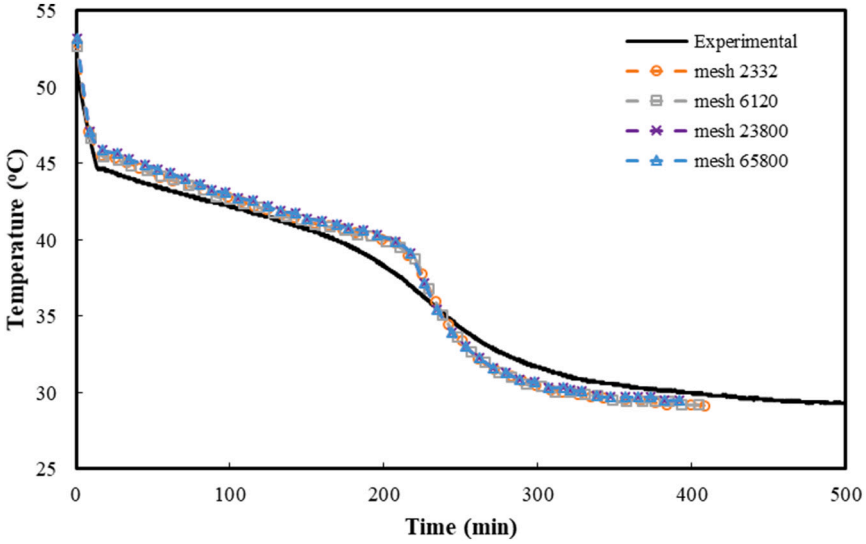

Fig. 10. Numerical cooling curves of the PCM using the enthalpy-porosity method.

the manufacturer, as detailed in Table 1. In the numerical simulation, a distinct abrupt change in the cooling curve is observed at the start and end points of solidification, occurring at 46 °C and 40 °C, respectively. In contrast, experimental values exhibit also an abrupt change when the first solid appears, but a much more gradual change in slope for the last. The computational effort required for the simulations was influenced significantly by the steep gradients in the source term, which necessitated high mesh resolution and iterative solver adjustments. For the enthalpy-porosity method, convergence was particularly challenging in regions where the source term exhibited abrupt changes from 0 to 10^8, requiring up to 80 iterations per time step. To mitigate these challenges, adaptive mesh refinement and solver preconditioning were employed, resulting in a computational time of approximately 12 h for a single simulation on cluster with 60 core process

Obviously, this is correspondence with the $c_p(T)$ curves seen in Fig. 2, in which the slope is almost infinite at the liquidus point but has moderate values further in the two-phase region and merges smoothly with the solid, even for very low cooling rates. Numerical results for the AHC method are shown in Fig. 11, again using manufacturer's values for the properties, except for heat capacity and viscosity, as explained above. Results using DSC measurements at the cooling rates of 1, 5, and 10 $^{\circ}C/min$ are shown.

It is observed that for the simulations with c_p determined at lower cooling rates, the results agree fairly in the region where the PCM is in the liquid phase and the phase change begins, and also well inside the two-phase region, but the same does not happen near the solidus point, the prediction shifting to the right with respect to the experimental curve. For data at higher cooling rates, initial fit is worse, in correspondence with Fig. 2, but agreement in the solid region improves.

Fig. 12 displays a comparison of the results for the cooling process using the enthalpy-porosity method, AHC method (at cooling rates of 1 $^{\circ}C/min$), and the experimental data. Although there is difference between the experimental results and both simulation techniques, the $c_p - T$ method demonstrates greater compatibility with the experimental data. Additionally, unlike the enthalpy-porosity method, the $c_p - T$ method does not exhibit a sudden shift in the mushy zone. This implies that the $c_p - T$ method provides more accurate predictions of the results. Furthermore, the results have been compared with those of Baze et al. [52] and Buruzs et al. [53], who proposed that the phase transition of PCMs is modeled using temperature-dependent specific heat capacities. These capacities are imported as cubic Hermite spline functions from the solid-liquid phase change material, and the approach is implemented through a User-Defined Function (UDF) in Fluent. This method shows a strong agreement with the enthalpy-porosity method, so that issues with compatibility with our experimental results logically ensue. While this study focuses on a single case, the two methods are widely utilized in

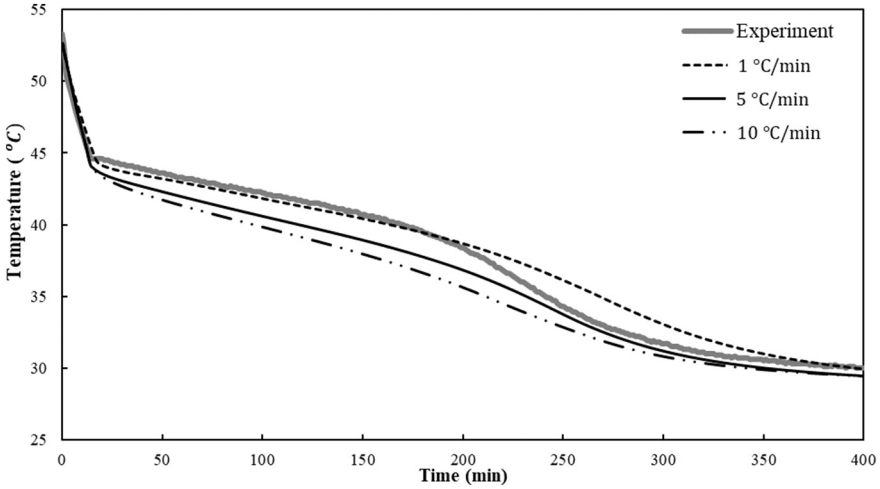

Fig. 11. Numerical cooling curves of the PCM using the AHC method for $c_p(T)$ curves at different DSC cooling rates.

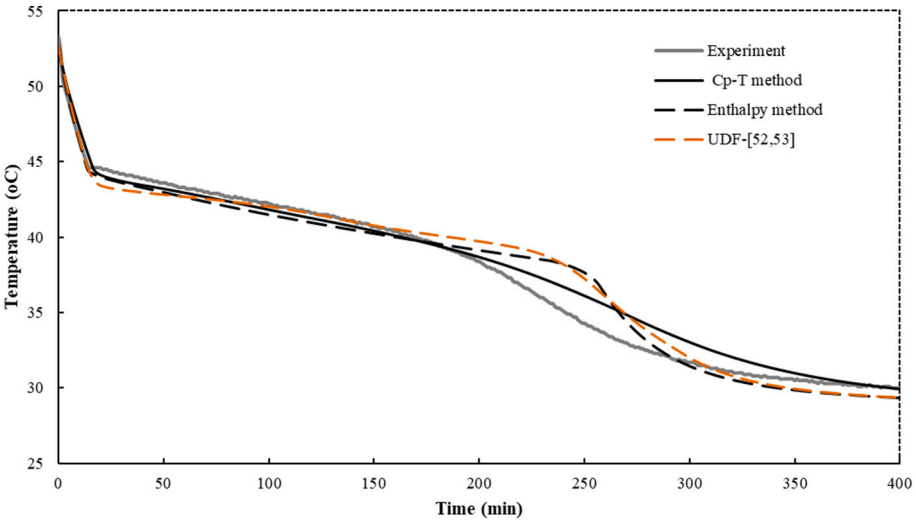

Fig. 12. Comparison of predicted cooling curves by different phase change models.

PCM modeling, and their fundamental principles extend beyond any specific case. The $c_p - T$ -based method, reliant on experimental $c_p - T$ curves, tends to be system-specific but is highly effective for systems where such data is available. In contrast, the enthalpy-based method offers greater physical robustness, enabling it to address a broader range of phase change phenomena and making it more versatile. These characteristics are independent of the specific experimental setup, which supports the possibility of generalizing our observations

As pointed out by several studies [5,54] the enthalpy-porosity method cannot be arranged via internal parameters nor properties to accurately reproduce the heating/cooling curve. In our case, it predicts an abrupt end of the phase change near the solidus point which greatly anticipates the solid cooling, all of which is absent in measurements. Meanwhile, the error is noticeably smaller with the AHC method, which can effectively predict the initial and final stages of solidification. However, it tends again to struggle with accurately simulating the solidus point.

Based on Fig. 11, the simulation results for a cooling rate of 1 °C/*min* exhibit good agreement with the experimental data for temperatures exceeding 39 °C. Conversely, for a cooling rate of 5 °C/*min*, satisfactory compliance is observed for temperatures below 34.6 °C. To mitigate the mismatch between simulation and experimental data within this range, an artificial $c_p - T$ curve is faired using an interpolation method. In the initial step, linear interpolation is implemented for temperatures falling within the range of 34.6–39 °C. Outside of this range, the previous profiles remain unchanged.

$$c_p = \begin{cases} c_p \ for\ 5^{\circ}\mathrm{C}/min & if\ 34.6 < T_s \\ linear\ interpolation & if\ 34.6 < T < 39 \\ c_p \ for\ 1^{\circ}\mathrm{C}/min & if\ T > 39 \end{cases} \quad (8)$$

Another approach is to calculate the average between $c_p - T$ curves obtained for cooling rates of 1 °C/*min* and 5 °C/*min*. This method aims to create a blended curve that incorporates characteristics from both cooling rates, potentially reducing discrepancies between simulation and experimental data across a wider temperature range. Both modified curves are shown in Fig. 13.

Fig. 14 shows numerical simulations for both modified c_p curves. The linear modification method produces results that closely match the cooling rate of 1 $^{o}C/min$, with some adjustments noted in the mushy zone. Notably, there is an alignment with experimental data in the liquid phase. However, it's important to highlight that the data for specific heat capacity in the solid phase was derived from a cooling rate of 5 $^{o}C/min$, resulting in a lack of similarity with the temperature profile observed for 5 $^{o}C/min$. For the second modification, where the average specific heat capacity is used, the resulting temperature profile closely resembles that of the 5 $^{o}C/min$ cooling rate. While the graph exhibits compatibility with

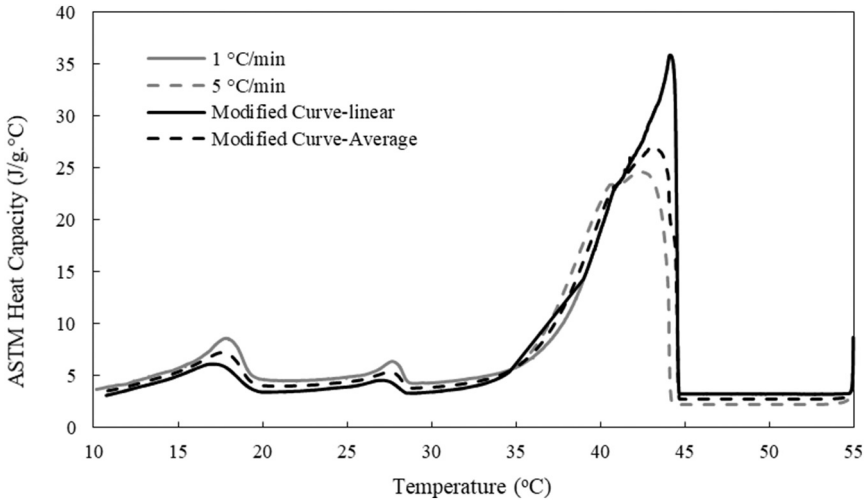

Fig. 13. Modified curves of specific heat capacity

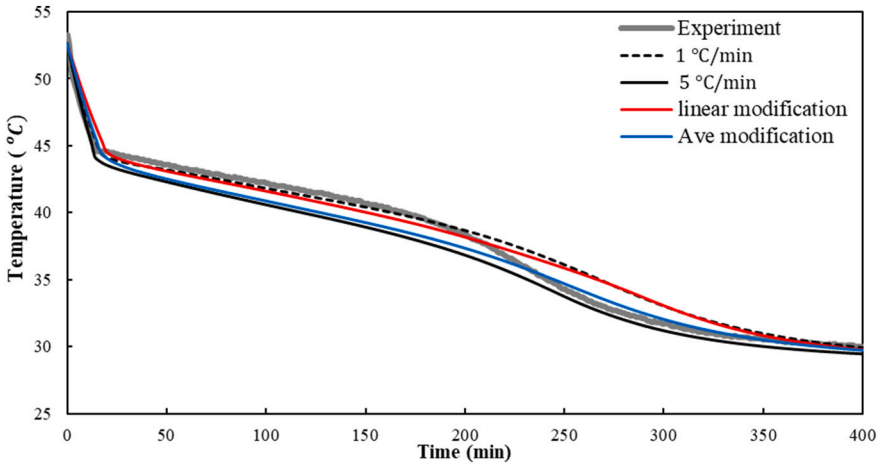

Fig. 14. Comparison of temperatures estimated by modified c_p values.

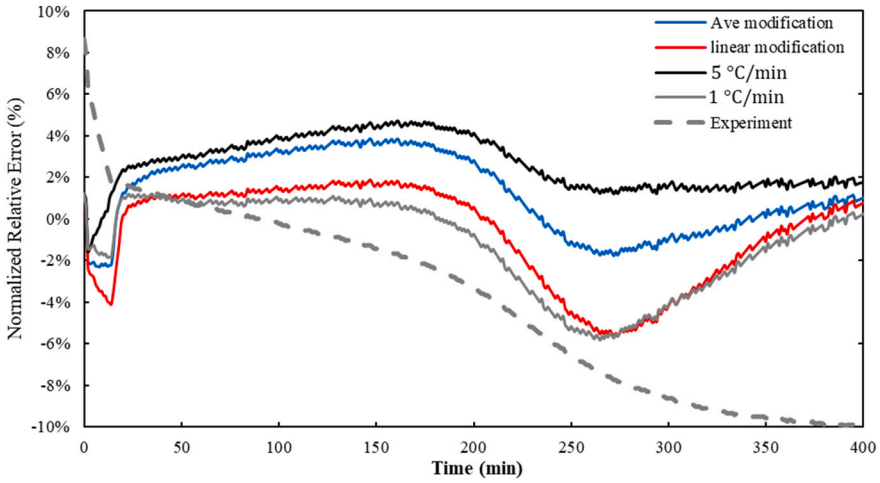

Fig. 15. Relative error curves for the AHC method, with c_p curves of 1 $^oC/min$, 5 $^oC/min$, linear modification and average modification

the 5 $^oC/min$ cooling rate in the liquid phase, discrepancies are apparent in the mushy zone and solid phase. However, despite these disparities, the modified profile closely approximates the experimental results. Indeed, both modified curves demonstrate improved accuracy and contribute to reducing the discrepancy between experimental and simulation data. These modifications refine the temperature profiles and enhance alignment with experimental observations, thereby improving the overall reliability and validity of the simulation results.

To express the discrepancy between a computed value and the true value, the graphs of normalized relative error (NRE) are presented in Fig. 15. The formula to calculate NRE is:

$$\mathrm{NRE} = \frac{T_{Sim} - T_{exp}}{0.5 \times (T_{Sim} + T_{exp})} \times 100 \tag{9}$$

where T_{Sim} simulation temperature and T_{exp} is experimental temperature. The results indicate that the relative error for the 1 $^oC/min$ cooling rate in the liquid phase is lower than that of the 5 $^oC/min$ cooling rate, but the opposite trend is observed for the solid phase. However, both modification methods lead to improvements in simulation results, with reductions in relative error observed. To quantify the error across all cases, the Root Mean Square Error (RMSE) has been utilized.

$$\mathrm{RMSE} = \sqrt{\frac{1}{n}\sum_{i=1}^{n}(y_i - \hat{y}_i)^2} \tag{10}$$

Table 2
The RMSE of the relative error graph

Specific heat profile used for simulation	RMSE
1 $^oC/min$	0.77
5 $^oC/min$	1.04
Linear modification	0.74
Average modification	0.8

where y_i is experimental data and $\hat{y}_i$ is simulation and n is number of observations. Since RMSE squares the errors, larger errors have a disproportionately greater impact on the metric. A low RMSE indicates that the model's predictions are closely aligned with the actual values, reflecting higher accuracy. As illustrate in Table 2, The linear modification method exhibits lower error and demonstrates the best compatibility with the experimental data, although the error is not significantly different from that of the 1 $^oC/min$cooling rate.Another intriguing observation is that despite the temperature profile of the average modification closely resembling that of the 5 $^oC/min$ cooling rate, the RMSE of the average modification is remarkably less than it.

Finally, it is also obvious that in real applications, large scales and quicker heat transfer are present, so that the effective application of the AHC method would require some previous knowledge about the situation to be modeled, predicted or simulated. In this respect, Fig. 16 indicates the rate of cooling calculated from the experimental

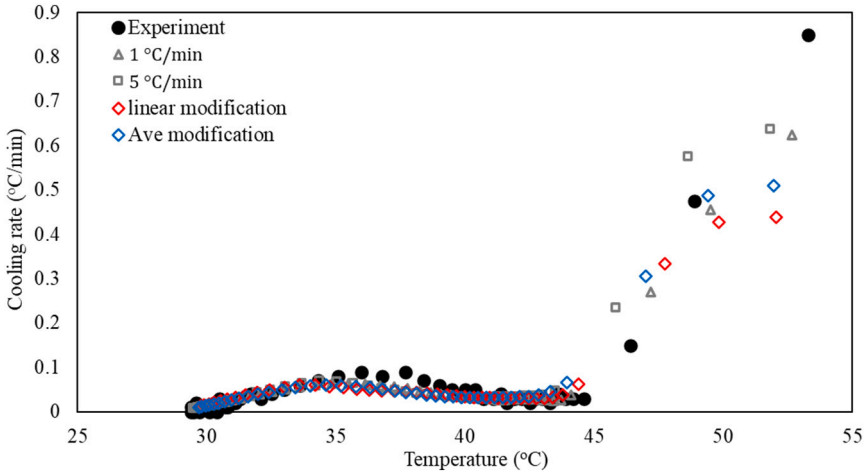

Fig. 16. Cooling rate of the experiment and comparison with simulations

temperatures and for the different numerical predictions. All simulations compare very well between them and with experiment. From the graph, it can be said that cooling rate is high for the liquid and decreases steeply as the first solid appears and natural convection apparently stops. It exhibits and almost constant value through the mushy region up to the point the last liquid disappears.

However, values obtained are extremely low, with a maximum below 0.9 $^{\circ}C/min$ and a minimum below 0.1, which have nothing to do whatsoever with conditions of the DSC measurements and the $c_p(T)$ curves used for the simulations. Obviously, a $c_p(T)$ curve at these speeds will exhibit higher peak and slope and thus larger disagreement with experimental measurements, as can be deduced from Figs. 2 and 11. Thus such a simple interpretation of the AHC method is flawed, and care must be exerted when numerically modeling PCM systems

5. Conclusions

Solidification under T-history conditions of a paraffin-type PCM enclosed in a vertical test tube has been numerically modeled, and predictions compared with temperatures determined experimentally. Two customary fixed-grid techniques have been used for liquid-solid phase change, the so-called enthalpy-porosity and the Apparent Heat Capacity (AHC) methods. The primary aim of this research is to enhance the reliability and efficiency of thermal storage systems by improving the predictive modeling of phase change processes. The insights gained from this study can guide the selection of modeling approaches for designing PCM-based thermal storage systems, particularly in applications where accurate predictions of thermal behavior are crucial.

Neither of the two is able to predict the cooling curves with an excellent agreement. The first (enthalpy-porosity) fails in modeling the disappearance of the last liquid, predicting a sharp change of slope that doesn't occur for these materials. The AHC performs far much better, at least with a gradual solidus transition, although a noticeable discrepancy persists. The essential shortcoming of this method is that one has to choose beforehand at which heating rate the $c_p(T)$ curve of the material has to be determined. In this respect, handling of practical problems can be tricky, because the speed of the DSC determinations seems to be amply disconnected from what happens in the experimental or practical system. Care is advised, as well as examination of the trend exhibited by the results with data at different DSC speeds. When comparing the two methods in terms of practical applications, the $c_p - T$ -based method is more suitable when experimental data is abundant, system calibration is feasible, and the material/system is well-characterized. On the other hand, the enthalpy-based method is preferable for modeling complex phase change processes, exploring new PCM materials, or when detailed experimental data is limited.

Nomenclature

c_p	specific heat $(J/kg.K)$
C	mushy zone constant (kg/m^2)
h	convection heat transfer $(W/m^2.K)$
H	enthalpy $(kg\ m^2 s^{-1})$
k	*thermal* conductivity $(W/m.K)$
L	latent heat of fusion (kJ/kg)
r	tube radius (m)
Ra	Rayleigh number
R	thermal resistance
t	time
T	Temperature (^oC)

Greek letters

β	volumetric expansion coefficient
γ	liquid volume fraction
ε	emissivity
μ	fluid viscosity $(kg\ m^{-1}s^{-1})$
ρ	fluid density (kgm^{-3})

Subscripts

conv	convection
g	glass
i	insulation
l	liquid phase
m	main peak
s	solid phase
rad	radiation

CRediT authorship contribution statement

Milad Tajik Jamal-Abad: Visualization, Software, Methodology, Investigation, Formal analysis, Conceptualization, Writing – original draft. **Arnold Martínez:** Validation, Data curation, Writing – review & editing. **Mauricio Carmona:** Resources, Data curation. **Cristóbal Cortés:** Validation, Supervision, Project administration, Data curation, Conceptualization, Writing – review & editing.

Declaration of competing interest

The authors declare that they have no known competing financial interests or personal relationships that could have appeared to influence the work reported in this paper.

Acknowledgements

This research was partially supported by the R&D project Transición Ecológica en Areas Rurales-Ecological traNSition rUral aREas (ENSURE). Ref.: TED2021-131397B-100. MINISTERIO DE CIENCIA E INNOVACIÓN.

Data availability

Data will be made available on request.

References

[1] H. Zhang, J. Baeyens, G. Cáceres, J. Degrève, Y. Lv, Thermal energy storage: recent developments and practical aspects, Prog. Energy Combust. Sci. 53 (2016) 1–40, https://doi.org/10.1016/j.pecs.2015.10.003.
[2] I. Sarbu, A comprehensive review of thermal energy storage, Sustainability 10 (1) (2018) 191, https://doi.org/10.3390/su10010191.
[3] A. Kumar, R. Kumar, Enhancement and estimation of thermo-physical properties of organic-phase change materials (O-PCMs) and their applications in solar thermal technologies: a review, J. Energy Storage 101 (Part A) (2024) 113741, https://doi.org/10.1016/j.est.2024.113741.
[4] H. Togun, H.S. Sultan, H.I. Mohammed, A.M. Sadeq, N. Biswas, H.A. Hasan, R. Z. Homod, A.H. Abdulkadhim, Z.M. Yaseen, P. Talebizadehsardari, A critical review on phase change materials (PCM) based heat exchanger: different hybrid techniques for the enhancement, J. Energy Storage 79 (2024) 109840, https://doi.org/10.1016/j.est.2023.109840.
[5] M. Arnold Martínez, M. Carmona, C. Cortés, I. Arauzo, Experimentally based testing of the enthalpy-porosity method for the numerical simulation of phase change of paraffin-type PCMs, J. Energy Storage 69 (2023) 107876, https://doi.org/10.1016/j.est.2023.107876.
[6] A. Surya, R. Prakash, N. Nallusamy, Heat transfer enhancement and performance study on latent heat thermal energy storage system using different configurations of spherical PCM balls, J. Energy Storage 72 (Part D) (2023) 108643, https://doi.org/10.1016/j.est.2023.108643.
[7] J.H. Nazzi Ehms, R. De César Oliveski, L.A. Oliveira Rocha, C. Biserni, Theoretical and numerical analysis on phase change materials (PCM): a case study of the solidification process of erythritol in spheres, Int. J. Heat Mass Transf. 119 (2018) 523–532, https://doi.org/10.1016/j.ijheatmasstransfer.2017.11.124.
[8] M.M. Kenisarin, K. Mahkamov, S.C. Costa, I. Makhkamova, Melting and solidification of PCMs inside a spherical capsule: a critical review, J. Energy Storage 27 (2020) 101082, https://doi.org/10.1016/j.est.2019.101082.
[9] S. Motahar, A.A. Alemrajabi, R. Khodabandeh, Experimental study on solidification process of a phase change material containing TiO2 nanoparticles for thermal energy storage, Energy Convers. Manag. 138 (2017) 162–170, https://doi.org/10.1016/j.enconman.2017.01.051.
[10] A.M. Sefidan, M. Taghilou, M. Mohammadpour, A. Sojoudi, Effects of different parameters on the discharging of double-layer PCM through the porous channel, Appl. Therm. Eng. 123 (2017) 592–602, https://doi.org/10.1016/j.applthermaleng.2017.05.131.
[11] M. Tajik Jamal-Abad, C. Cortés, J. Pallarés Ranz, A. Gil, Approximate analytical solution for solidification of PCM in cylindrical geometry with temperature-dependent thermal conductivity—perturbation method, J. Phys. Conf. Ser. 2766 (2024) 012032, https://doi.org/10.1088/1742-6596/2766/1/012032.
[12] A. Peter, O. Cornelia, Study on solid-liquid interface heat transfer of PCM under simultaneous charging and discharging (SCD) in horizontal cylinder annulus, Heat Mass Transf. (2017), https://doi.org/10.1007/s00231-017-1971-1.
[13] A. Mohammadian Soodmand, S. Nejatbakhsh, H. Pourpasha, H. Aghdasinia, S. Zeinali Heris, Simulation of melting and solidification process of polyethylene glycol 1500 as a PCM in rectangular, triangular, and cylindrical enclosures, Alex. Eng. J. 61 (11) (2022) 8431–8456, https://doi.org/10.1016/j.aej.2022.02.011.
[14] M.Y. Shaker, A.A. Sultan, E.A. El Negiry, A. Radwan, Melting and solidification characteristics of cylindrical encapsulated phase change materials, J. Energy Storage 43 (2021) 103104.
[15] A.A.R. Darzi, M. Jourabian, M. Farhadi, Melting and solidification of PCM enhanced by radial conductive fins and nanoparticles in cylindrical annulus, Energy Convers. Manag. 118 (2016) 253–263, https://doi.org/10.1016/j.enconman.2016.04.016.
[16] R.A. Alsulami, T.M. Zope, K. Premnath, M. Aljaghtham, Convectively cooled solidification in phase change materials in different configurations subject to internal heat generation: quasi-steady analysis, Appl. Therm. Eng. 221 (2023) 119849.
[17] F. Afsharpanah, M. Izadi, F. Akbarzadeh Hamedani, S.S. Mousavi Ajarostaghi, W. Yaïci, Solidification of nano-enhanced PCM-porous composites in a cylindrical cold thermal energy storage enclosure, Case Stud. Therm. Eng. 39 (2022) 102421, https://doi.org/10.1016/j.csite.2022.102421.
[18] M. Mahamudur Rahman, H. Hu, H. Shabgard, P. Boettcher, Y. Sun, M. McCarthy, Experimental characterization of inward freezing and melting of additive-enhanced phase-change materials within millimeter-scale cylindrical enclosures, J. Heat Transf. 138 (2016) 1–13, https://doi.org/10.1115/1.4033007.
[19] H.F. Öztop, B. Kiyak, N. Biswas, F. Selimefendigil, H. Coşanay, Effects of cooler shape and position on solidification of phase change material in a cavity, J. Taiwan Inst. Chem. Eng. 163 (2024) 105628.
[20] M.H. Hekmat, M.H.K. Haghani, E. Izadpanah, H. Sadeghi, The influence of energy storage container geometry on the melting and solidification of PCM, Int. Commun. Heat Mass Transfer 137 (2022) 106237, https://doi.org/10.1016/j.icheatmasstransfer.2022.106237.
[21] B. Izgi, M. Arslan, Numerical analysis of solidification of PCM in a closed vertical cylinder for thermal energy storage applications, Heat Mass Transf. 56 (2020) 2909–2922, https://doi.org/10.1007/s00231-020-02911-z.
[22] Y. Allouche, S. Varga, C. Bouden, A. Oliveira, Validation of a CFD model for the simulation of heat transfer in a tubes-in-tank PCM storage unit, Renew. Energy 89 (2016) 371–379, https://doi.org/10.1016/j.renene.2015.12.010.
[23] J.N.W. Chiu, V. Martin, Multistage latent heat cold thermal energy storage design analysis, Appl. Energy 112 (2013) 1438–1445, https://doi.org/10.1016/j.apenergy.2013.02.018.
[24] A.H. Mosaffa, C.A. Infante Ferreira, F. Talati, M.A. Rosen, Thermal performance of a multiple PCM thermal storage unit for free cooling, Energy Convers. Manag. 67 (2013) 1–7, https://doi.org/10.1016/j.enconman.2012.10.007.
[25] W. Ye, D. Zhu, N. Wang, Fluid flow and heat transfer in a latent thermal energy unit with different phase change material (PCM) cavity volume fractions, Appl. Therm. Eng. 42 (2012) 49–57, https://doi.org/10.1016/j.applthermaleng.2011.12.016.
[26] S. Riahi, D. Whaley, S. Sheoran, D. Buddhi, F. Bruno, Numerical investigation of a PCM system for thermal management of large-scale battery installation in remote area power systems, Appl. Therm. Eng. 263 (2025) 125322, https://doi.org/10.1016/j.applthermaleng.2024.125322.
[27] S.M. Vahidhosseini, Z. Esmaeili, S. Rashidi, R. Rafee, W.-M. Yan, Effects of novel fins on PCM melting/solidification in triplex tube heat exchangers, Appl. Therm. Eng. 262 (2025) 125217, https://doi.org/10.1016/j.applthermaleng.2024.125217.
[28] A.C. Kheirabadi, D. Groulx, 'The effect of the mushy-zone constant on simulated phase change heat transfer', in: Proceedings of CHT-15 ICHMT International Symposium on Advances in Computational Heat Transfer, p. 22, 2015, https://doi.org/10.1615/ichmt.2015.intsympadvcomputheattransf.460.
[29] F.L. Rashid, A.F. Khalaf, H. Togun, A. Chattopadhyay, M.A. Al-Obaidi, B. K. Sharma, Investigating the impact of fin configuration on phase change material melting in square cells: a numerical study, J. Energy Storage 105 (2025) 114680, https://doi.org/10.1016/j.est.2024.114680.
[30] M. Iten, S. Liu, S. Shukla, P.D. Silva, Investigating the impact of C_p-T values determined by DSC on the PCM-CFD model, Appl. Therm. Eng. 117 (2017) 65–75, https://doi.org/10.1016/j.applthermaleng.2017.02.026.
[31] V.A.A. Raj, R. Velraj, Heat transfer and pressure drop studies on a PCM-heat exchanger module for free cooling applications, Int. J. Therm. Sci. 50 (2011) 1573–1582, https://doi.org/10.1016/j.ijthermalsci.2011.03.014.
[32] G. Diarce, A. Campos-Celador, K. Martin, A. Urresti, A. García-Romer, J.M. Sala, A comparative study of the CFD modeling of a ventilated active façade including phase change materials, Appl. Energy 126 (2014) 307–317, https://doi.org/10.1016/j.apenergy.2014.03.038.
[33] T. Barz, J. Krämer, J. Emhofer, Identification of phase fraction–temperature curves from heat capacity data for numerical modeling of heat transfer in commercial paraffin waxes, Energies 13 (2020) 5149, https://doi.org/10.3390/en13195149.
[34] A.C. Kheirabadi, D. Groulx, 'The effect of the mushy-zone constant on simulated phase change heat transfer', in: Proceedings of the CHT-15. 6th International Symposium on Advances in Computational Heat Transfer, p. 22. Begellhouse, 2015.
[35] M. Iten, S. Liu, A. Shukla, Experimental validation of an air-PCM storage unit comparing the effective heat capacity and enthalpy methods through CFD simulations, Energy 155 (2018) 495–503, https://doi.org/10.1016/j.energy.2018.04.073.
[36] C. Reichl, S. Both, P. Mascherbauer, J. Emhofer, Comparison of two CFD approaches using constant and temperature dependent heat capacities during the phase transition in PCMs with experimental and analytical results, Processes 10 (2) (2022) 302, https://doi.org/10.3390/pr10020302.
[37] A. El Ouali, Y. Khattari, B. Lamrani, T. El Rhafiki, Y. Zeraouli, T. Kousksou, Apparent heat capacity method to describe the thermal performances of a latent thermal storage system during discharge period, J. Energy Storage 52 (B) (2022) 104960, https://doi.org/10.1016/j.est.2022.104960.
[38] Y. Khattari, T. El Rhafiki, N. Choab, T. Kousksou, M. Alaphilippe, Y. Zeraouli, Apparent heat capacity method to investigate heat transfer in a composite phase change material, J. Energy Storage 28 (2020) 101239, https://doi.org/10.1016/j.est.2020.101239.
[39] ANSYS, FLUENT R2 User's Manual, ANSYS Inc., 2020.
[40] C. Castellón, E. Günther, H. Mehling, S. Hiebler, L.F. Cabeza, Determination of the enthalpy of PCM as a function of temperature using a heat-flux DSC: a study of different measurement procedures and their accuracy, Int. J. Energy Res. 32 (13) (2008) 1258–1265, https://doi.org/10.1002/er.1443.
[41] ASTM International, Standard Test Method for Measurement of Transition Temperatures of Petroleum Waxes by Differential Scanning Calorimetry (DSC) (ASTM D4419–21), Annual Book of Standards, West Conshohocken, PA, 2021.

[42] A. Martínez, M. Carmona, C. Cortés, I. Arauzo, Characterization of thermophysical properties of phase change materials using unconventional experimental technologies, Energies 13 (18) (2020) 4687, https://doi.org/10.3390/en13184687.
[43] ASTM International, Test method for determining specific heat capacity by differential scanning calorimetry (ASTM E1269-11R18), West Conshohocken, PA. (2018), https://doi.org/10.1520/E1269-11R18.
[44] F.P. Incropera, Fundamentals of Heat and Mass Transfer, 6th ed., Wiley, 2007.
[45] P.A. Galione, O. Lehmkuhl, J. Rigola, A. Oliva, Fixed-grid numerical modeling of melting and solidification using variable thermo-physical properties – application to the melting of n-octadecane inside a spherical capsule, Int. J. Heat Mass Transf. 86 (2015) 721–743, https://doi.org/10.1016/j.ijheatmasstransfer.2015.03.033.
[46] A. Solé, L. Miró, C. Barreneche, I. Martorell, L.F. Cabeza, Review of the T-history method to determine thermophysical properties of phase change materials (PCM), Renew. Sust. Energ. Rev. 26 (2013) 425–436, https://doi.org/10.1016/j.rser.2013.05.023.
[47] V.R. Voller, M. Cross, N.C. Markatos, An enthalpy method for convection/diffusion phase change, Int. J. Numer. Methods Eng. 24 (1987) 271–284, https://doi.org/10.1002/nme.1620240207.
[48] S.N. Al-Saadi, Z. Zhai, Modeling phase change materials embedded in building enclosure: a review, Renew. Sust. Energ. Rev. 21 (2013) 659–673.
[49] A. Caggiano, C. Mankel, E. Koenders, Reviewing theoretical and numerical models for PCM-embedded cementitious composites, Buildings 9 (2019) 3.
[50] S. Arun Prakash, C. Hariharan, R. Arivazhagan, R. Sheeja, Antony Aroul Raj, V. & Velraj, R., Review on numerical algorithms for melting and solidification studies and their implementation in general purpose computational fluid dynamic software, J. Energy Storage 36 (2021) 102341, https://doi.org/10.1016/j.est.2021.102341.
[51] D.K. Gartling, In K. Morgan, C. Taylor & C.A. Brebbia (Eds.), Computer Methods in Fluids, Pentech, 1980, pp. 219–230.
[52] T. Barz, A. Bres, J. Emhofer, slPCMlib: a Modelica library for phase change materials, Proc. Asian Model. Conf. 2022 (2022) 63–74.
[53] A. Buruzs, F. Giordano, M. Schieder, C. Reichl, M. Goderis, W. Beyne, M. De Paepe, T. Barz, CFD simulation of solid/liquid phase change in commercial PCMs using the slPCMlib library, J. Phys. Conf. Ser. 2766 (2024) 012223, https://doi.org/10.1088/1742-6596/2766/1/012223.
[54] W.-B. Ye, M. Arıcı, Exploring mushy zone constant in enthalpy-porosity methodology for accurate modeling convection-diffusion solid-liquid phase change of calcium chloride hexahydrate, Int. Commun. Heat Mass Transfer 152 (2024) 107294, https://doi.org/10.1016/j.icheatmasstransfer.2024.107294.